Electronic Supplementary Information

Nano-sized NaF inspired intrinsic solvothermal growth mechanism of rare-earth nanocrystals for facile control synthesis of high-quality and small-sized hexagonal $NaYbF_4$:Er

Jiwei Shen,*[a] Zhiqing Wang,[a] Jiawei Liu[a] and Hua Li*[b,c]

[a] Key Laboratory of Synthetic and Natural Functional Molecule Chemistry of the Ministry of Education. College of Chemistry & Materials Science, Northwest University, Xi' an 710069, People's Republic of China;

[b] Institute of Analytical Science, College of Chemistry & Material Science, Northwest University, Xi'an 710069, China;

[c] College of Chemistry and Chemical Engineering, Xi'an Shiyou University, Xi'an 710065, China.

Table S1 Elemental analysis results of the NaF nanoparticles shown in Fig. 1D as detected during element mapping analysis.

Element	Line Type	Wt%	Atomic%
Na	K series	47.16	40.18
F	K series	43.44	44.81
C	K series	8.59	14.03
O	K series	0.80	0.98
N	K series	0.00	0.00
Total:		100.00	100.00

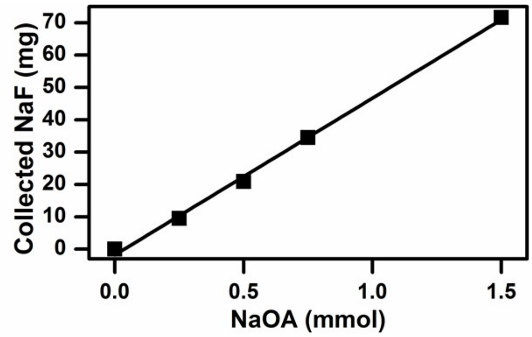

Fig. S1 Plot of mass of the collected NaF against the amount of NaOA reactant for the NaOA-NH_4F reaction in methanol. The NaOA transformed to NaF completely according to a stoichiometric ratio of 1:1 at low NaOA concentration, however, the mass of collected NaF slightly exceeded its theoretical value at higher NaOA concentration likely due to the absorption of ammonium oleate.

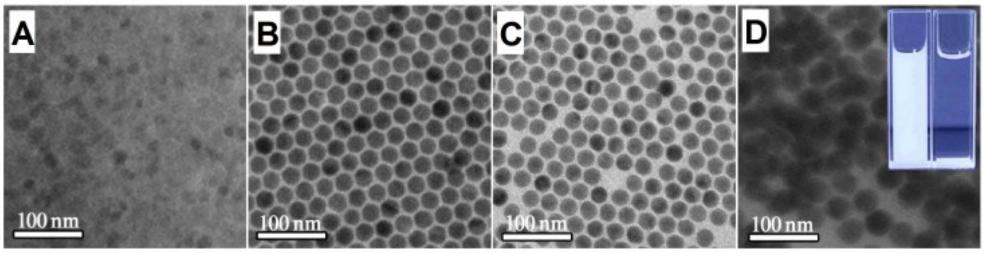

Fig. S2 TEM images: NaOA-HOA-ODE (A); $NaLuF_4$:Yb/Er prepared by using NaOA strategy under the Na/RE/F ratio of 2.5:1:4 (B); 3.5:1:4 (C) and 5:1:4 (D). Inset of (D): corresponding digital photo of the aggregated UCNCs dispersed in cyclohexane before (left) and after (right) HOA washing. Uniform and small-sized β-$NaLuF_4$:Yb/Er could be achieved under lower NaOA/Re (2.5:1, 3.5:1), however, further increased NaOA/Re (5:1) resulted in uniform but unexpected larger and aggregated β-$NaLuF_4$:Yb/Er (Figure S2B-D). There seemed to be a threshold NaOA amount above which the β-phase nucleation was markedly suppressed. Much higher pH (~8) of the aggregated UCNCs (0.1 M in cyclohexane) than that of previous monodisperse samples (~6), and TEM image of the aggregated UCNCs (Figure S2D) reminded us there should be NaOA absorbed onto them. Few milliliters of HOA were added to dissolve the aggregated UCNCs, followed by ethanol/cyclohexane purification procedures. The aggregated UCNCs became transparent and monodisperse in cyclohexane (Figure S2D, inset), and much less in volume (Figure S3), confirming the presence and successful removal of NaOA on the aggregated UCNCs via the HOA-NaOA reaction.

Fig. S3 Digital photo of the aggregated $NaLuF_4$:Yb/Er dispersed in ethanol/cyclohexane before (left) and after (right) HOA washing. Solid products were obtained by centrifugation.

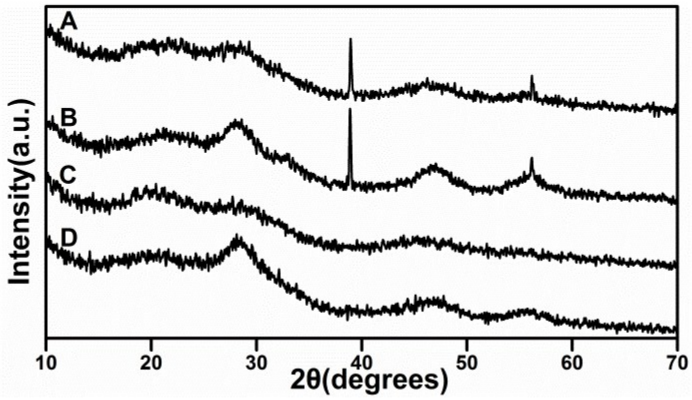

Fig. S4 XRD patterns of the samples collected at 150 °C (0 min). NaOH strategy: (A) $NaYF_4$:Yb/Er, (B) $NaYbF_4$:Er; NaOA strategy: (C) $NaYF_4$:Yb/Er, (D) $NaYbF_4$:Er.

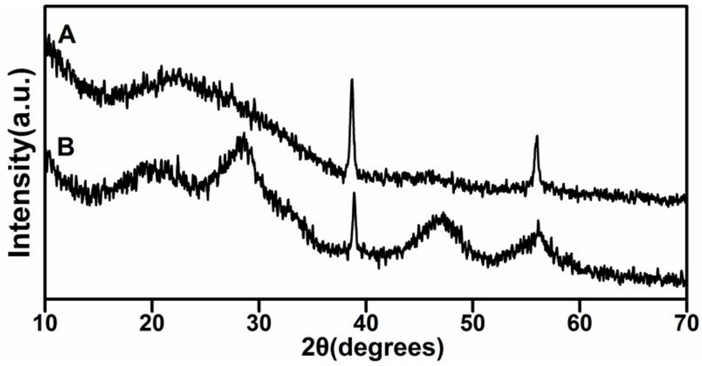

Fig. S5 XRD patterns of the samples prepared by using NaOA strategy and collected at 200 °C (0 min): (A) $NaYF_4$:Yb/Er, (B) $NaYbF_4$:Er.

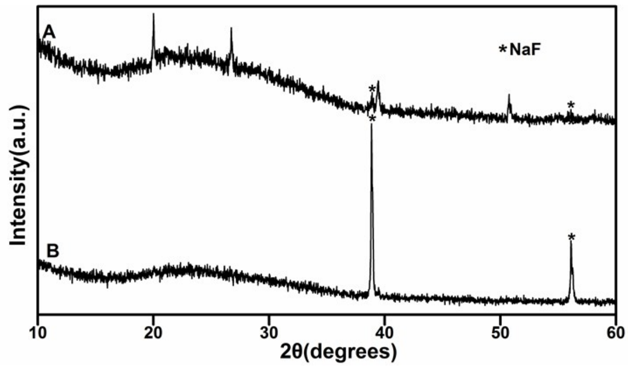

Fig. S6 XRD patterns: (A) the product of tail gas-NaOH reaction in NaOA based NaYbF$_4$:Er synthesis; (B) the product of NaOH treated waste methanol. The waste methanol was obtained after about twenty times of NaOA based synthesis. Both products were collected by centrifugation, washed with CH$_3$OH and dried before XRD analysis.

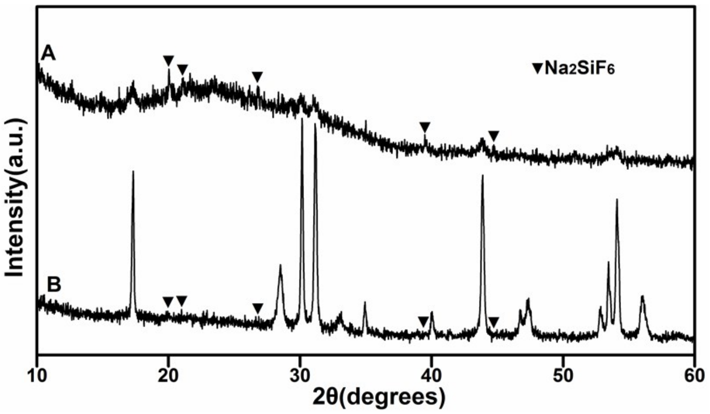

Fig. S7 System HF level characterization by XRD analysis of the HF-SiO$_2$ reaction products. The samples used in (A) and (B) were prepared according to the following procedures. (A) The NaOA based NaYbF$_4$:Er synthesis system was cooled to room temperature as soon as the reaction temperature reached 300 °C, followed by removing most of the nanocrystals via centrifugation, heating the resultant solution at 300 °C for 30 min, and then cooled down. Direct centrifugation was used to collect the reaction products. (B) The NaOH based NaYbF$_4$:Er synthesis system was cooled to room temperature as soon as the reaction temperature reached 300 °C, followed by removing most of the nanocrystals via centrifugation, heating the resultant solution at 300 °C for 30 min, and then cooled down. Direct centrifugation was also used to collect the reaction products. Nanocrystal removing steps were designed to decrease the HF consumption in the growth UCNCs, and thus the system HF level could be reflected by the products of subsequent HF-SiO$_2$ etching reaction at 300 °C. Results demonstrated there was more HF-SiO$_2$ product of Na$_2$SiF$_6$ in sample (A) than that of in sample (B), indicating the HF level in actual NaOA based system was higher than that of in NaOH based one.

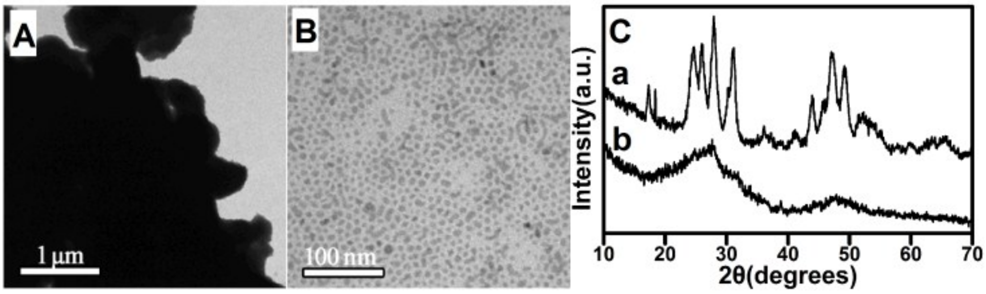

Fig. S8 TEM images of RE(OA)$_x$F$_y$ prepared by heating RE(OA)$_3$/NH$_4$F/HOA/ODE mixture (RE=Y^{3+}, Yb^{3+}, respectively) at 300 °C for 10 min: (A) YF$_3$; (B) Yb(OA)$_x$F$_y$. (C): (a) and (b) are XRD patterns of the samples used in (A) and (B), respectively. The nucleation efficiency of α-NaYbF$_4$:Er was higher than that of α-NaYF$_4$:Yb/Er since NaF was consumed up in NaOH based NaYbF$_4$:Er synthesis at 290 °C but there was still residual NaF in NaOH based NaYF$_4$:Yb/Er synthesis (Fig. 6A). However, higher α-nucleation efficiency did not provide higher α-to-β transition efficiency (Fig. 2A *vs* Fig. 2B). Loose-orthorhombic YF$_3$ formed by accumulation of tiny nanoparticles in Y(OA)$_3$-NH$_4$F reaction (Figure S8A). The YF$_3$ had low dispersity in cyclohexane, showing weak binding capacity of Y^{3+}, and most OA$^-$ of Y(OA)$_3$ was removed by F$^-$, leading to crosslinking Y^{3+}-F$^-$-Y^{3+} reaction. By contrast, the NH$_4$F-Yb(OA)$_3$ reaction gave monodisperse Yb(OA)$_x$F$_y$ nanoparticles (Figure S8B), showing such reaction did not remove OA$^-$ completely. Results demonstrated stronger binding capacity of Yb^{3+} than that of Y^{3+}.

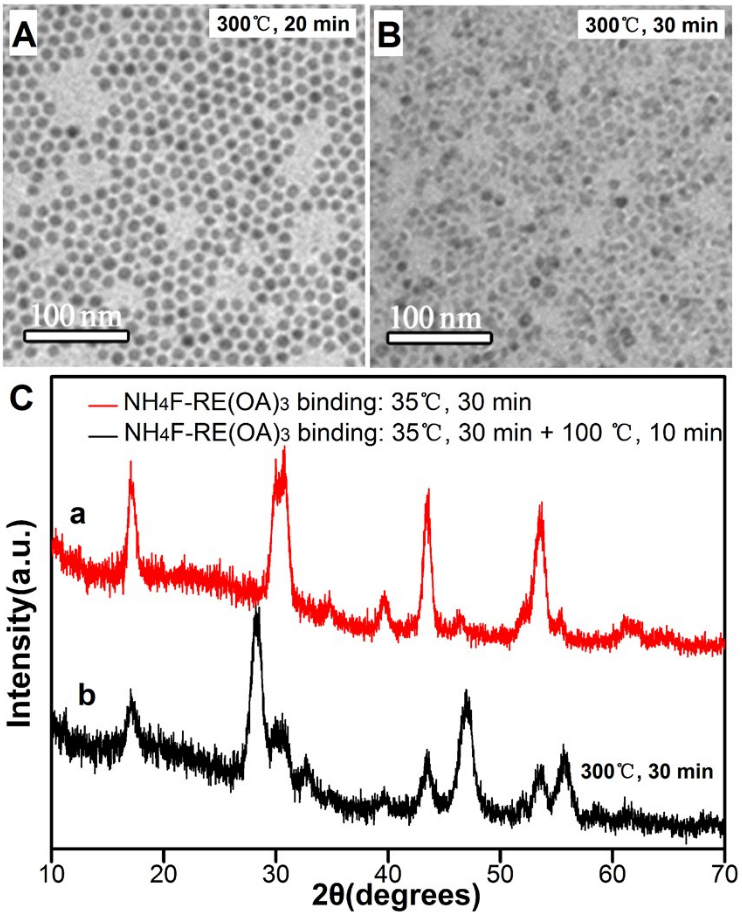

Fig. S9 TEM images of $NaYF_4$:Yb/Er prepared by adding NH_4F ahead of NaOH: (A) NH_4F-$RE(OA)_3$ binding was performed at 35 °C for 30 min and high temperature reaction was performed at 300 °C for 20 min; (B) NH_4F-$RE(OA)_3$ binding was performed at 100 °C for 10 min after binding at 35 °C for 30 min and high temperature reaction was performed at 300 °C for 30 min. (C) (a) and (b) are XRD patterns of the samples used in (A) and (B), respectively. Results indicated delayed α-to-β transition and less β-$NaREF_4$ nuclei by using the strengthened NH_4F-$RE(OA)_3$ binding strategy.

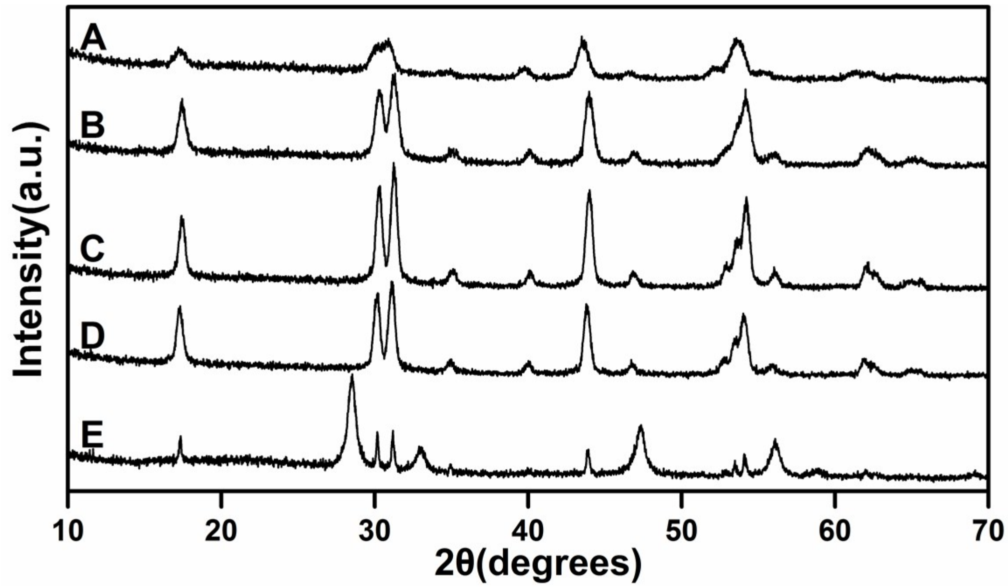

Fig. S10 XRD patterns of the as-prepared $NaYbF_4$:Er by the proposed binary sodium strategy and different NaOH/NaOA ratio: (A) 0:60, (B) 3:57, (C) 4.5:55.5, (D) 6:54, (E) 12:48.

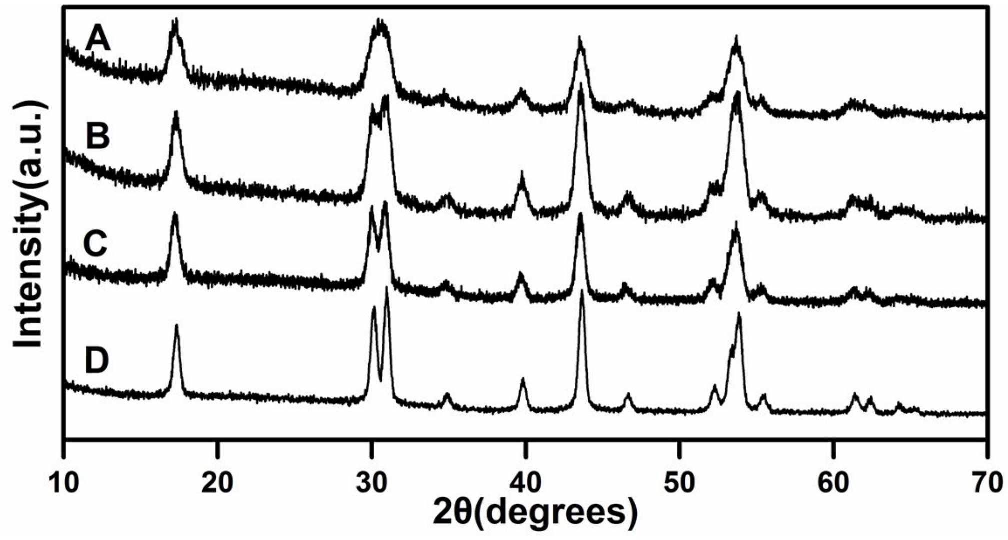

Fig. S11. XRD patterns of the as-prepared $NaYF_4$:Yb/Er by the proposed binary sodium strategy and different NaOH/NaOA ratio: (A) 0:60, (B) 9:51, (C) 12:48, (D) 15:45.

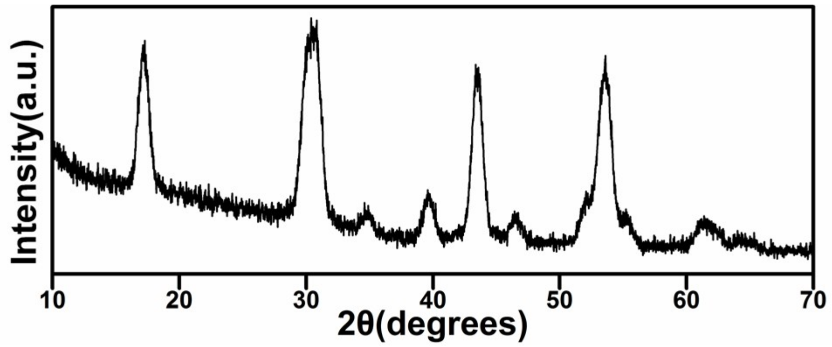

Fig. S12 XRD patterns of the as-prepared $NaYF_4$:Yb/Er by the proposed binary sodium strategy (Na/RE/F=3.5:1:4, NaOH/NaOA = 6:78).

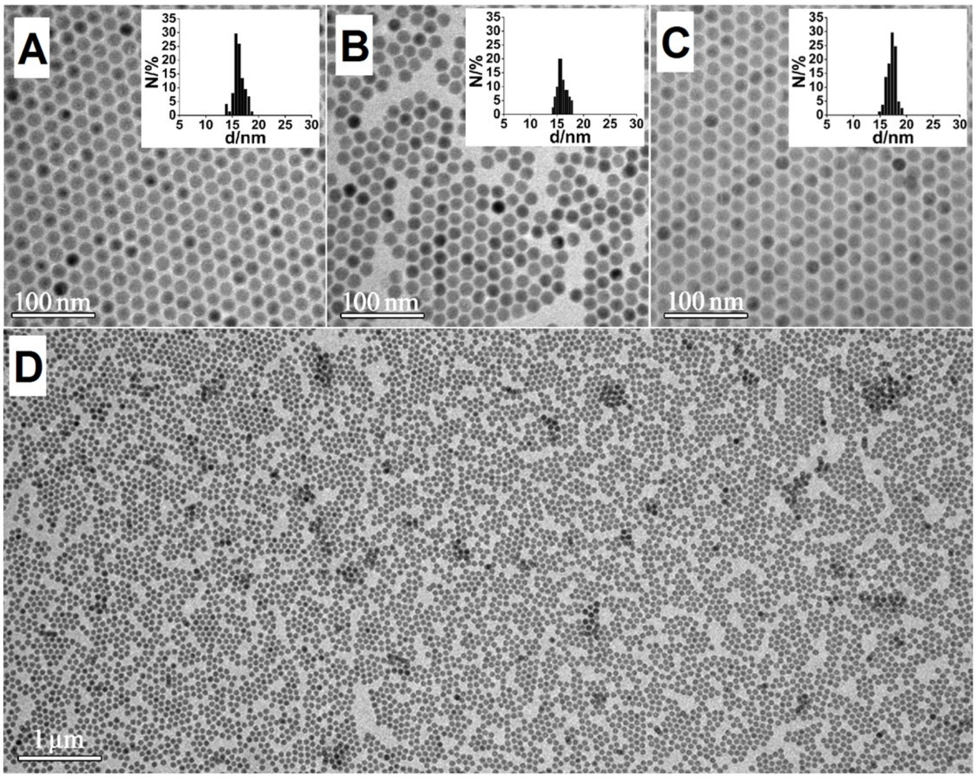

Fig. S13 TEM images of $NaYF_4$:Yb/Er prepared by the proposed binary sodium strategy (Na/RE/F=2.5:1:4, NaOH/NaOA = 12:48) at 300 °C for 1 h. The synthesis conditions were the same for the samples used in (A)-(C). (D) A typical overview TEM image for the sample used in (B). The diameters were 16.2 nm ± 6.2%, 16.1 nm ± 5.5% and 16.8 nm ± 5.5% for the sample used in (A), (B) and (C), respectively. The diameter relative standard deviation was only 3.8% for these three samples, demonstrating the proposed binary sodium strategy provided excellent nanocrystal size reproducibility.

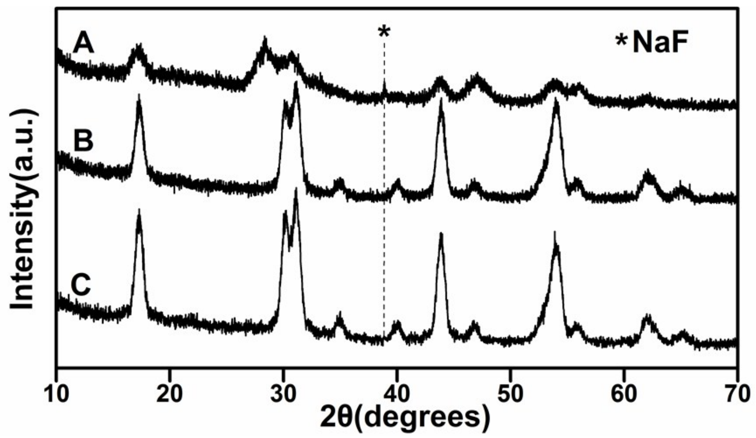

Fig. S14 XRD patterns of NaYbF$_4$:Er prepared by using NaOA strategy (Na/RE/F=2.5:1:4, 300 °C) and different reaction time: (A) 10 min; (B) 20 min; (C) 30 min.

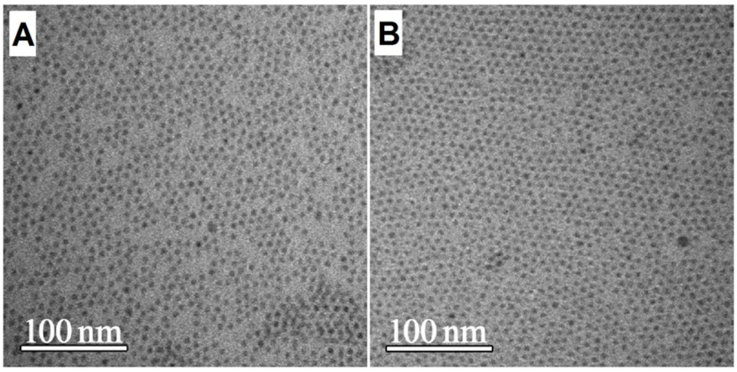

Fig. S15 TEM images of NaYF$_4$:Yb/Er prepared by using NaOA strategy (Na/RE/F= 2.5:1:4, 300 °C) and different reaction time: (A) 10 min, (B) 20 min.

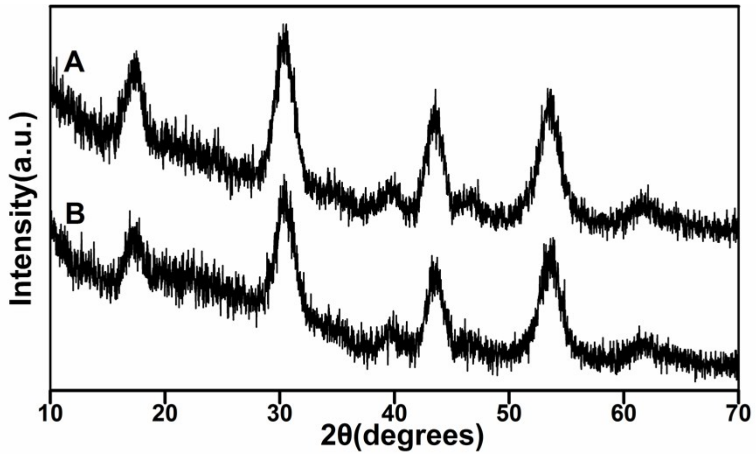

Fig. S16 XRD patterns of NaYF$_4$:Yb/Er prepared by using NaOA strategy (Na/RE/F= 2.5:1:4, 300 °C) and different reaction time: (A) 10 min, (B) 20 min.